HHS Public Access

Author manuscript

Adv Healthc Mater. Author manuscript; available in PMC 2017 September 06.

Published in final edited form as:

Adv Healthc Mater. 2017 September ; 6(17): . doi:10.1002/adhm.201700162.

Multifunctional Polymeric Micelles for Combining Chelation and Detection of Iron in Living Cells

Dr. Zhi Liu,
Department of Pharmaceutical & Biomedical Sciences, College of Pharmacy, University of Georgia, Athens, GA 30602-2352, USA

Max Purro,
Department of Pharmaceutical & Biomedical Sciences, College of Pharmacy, University of Georgia, Athens, GA 30602-2352, USA. Pharmaceutical Sciences Division, School of Pharmacy, University of Wisconsin–Madison, Madison, WI 53705-2222, USA

Dr. Jing Qiao, and
Department of Pharmaceutical & Biomedical Sciences, College of Pharmacy, University of Georgia, Athens, GA 30602-2352, USA

Prof. May P. Xiong
Department of Pharmaceutical & Biomedical Sciences, College of Pharmacy, University of Georgia, Athens, GA 30602-2352, USA

Abstract

Multifunctional self-assembled micelles composed of Pluronics F127 polymer chains are developed and investigated for chelation and selective detection of iron(III) in vitro and in iron-overloaded cells. Tetraphenylethene (TPE) is encapsulated into the micelle core and the iron chelate drug deferoxamine (DFO) is conjugated to micelles to generate a fluorescence quenching detection system termed DFO-TFM for short, where T stands for TPE, F for F127, and M for micelle. The key to the successful formation of this fluorescence quenching system is due to the near-ideal overlap between the absorption spectrum of the DFO:iron(III) complex and fluorescence spectrum of TPE. DFO-TFM can retain the iron-chelation properties of DFO and exhibits negligible cytotoxicity compared to free DFO. Furthermore, this fluorescence “turn-off” system can be utilized to detect the presence of iron and to monitor the chelation process in an iron overload cell model. This study serves as an effective proof-of-concept model for designing future in vivo systems capable of combining the features of iron chelation with iron detection and efforts toward the development of such detection systems are currently underway.

Correspondence to: May P. Xiong.
The ORCID identification number(s) for the author(s) of this article can be found under https://doi.org/10.1002/adhm.201700162.

Conflict of Interest
The authors declare no conflict of interest.

Supporting Information
Supporting Information is available from the Wiley Online Library or from the author.

Keywords

chelation; deferoxamine; iron overload; micelles; sensors

Iron overload can cause irreversible oxidative damage to cells and tissues, and is associated with numerous conditions such as neuroinflammation and progression of Alzheimer and Parkinson's disease.[1,2] Due to the body's inability to efficiently protect cells against iron overload, metal chelators are often employed to remove surplus iron, of which the most commonly used drug is deferoxamine (DFO).[3,4] One critical drawback of DFO therapy relates to its severe neurotoxicity at high doses,[5] which can be addressed through the development of nanomaterial–drug conjugates with minimal effect on the iron chelation efficiency of the drug.[6–8] Unfortunately, the degree of iron chelation cannot be controlled during DFO therapy and since iron plays a crucial role in a variety of vital cell functions, it is critical to avoid removing too much iron from the body. As a result, the development of a safe and effective tool capable of both chelating iron and monitoring this process would be quite informative in helping doctors make subsequent health care decisions when treating patients with DFO. Recently, fluorescent sensors have been widely investigated for their capabilities to provide sensitive and selective information to monitor iron.[9–11] Although excess iron usually ends up being stored in ferritin to maintain the balance of iron in the body,[12] current fluorescent probes have mainly been developed to selectively detect exogenous iron(III) in live cells and do not reflect the actual state of iron overload.[11] Furthermore, the poor solubility and high toxicity of these small-molecule fluorescent probes in aqueous media also hamper their practical applications.

Polymeric micelles from amphiphilic block copolymers have attracted considerable attention due to their unique characteristics such as high water-solubility, facile surface functionalization, and low toxicity.[13–15] The unique architecture of polymeric micelles allows for the incorporation of multiple functional components within a single micelle.[16–18] In this study, we have shown that mixed micelles comprised of F127 and F127–DFO polymer conjugates can encapsulate tetraphenylethylene (TPE) (Figure 1). TPE fluoresces, due to an aggregation-induced state in the micelle, can be quenched in the presence of iron in a manner proportional to the degree of DFO:iron(IIII) complexation. By engineering the iron chelating drug and the iron-selective "on–off" fluorescent module into the final structure of polymeric micelles, we were able to monitor the chelation process in an iron-overload live cell model.

With the exception of a few modifications, F127—$(COOH)_2$ was synthesized as previously reported[19] and DFO was then covalently conjugated via amide linkage to the terminal ends of the polymer via EDC/HOBt (1-ethyl-3-(3-dimethylaminopropyl)-carbodiimide/ Hydroxybenzotriazole) coupling methods to yield the final F127–$(DFO)_2$ conjugate (Figure S1, Supporting Information). A new peak assigned to the —OCH_2COOH— protons (δ = 3.98 ppm) can be easily observed in the spectra of F127—$(COOH)_2$ and validates the successful conversion of terminal —OH groups to —COOH (Figure S2A, Supporting Information). Subsequently, the peak assigned to these protons at δ 3.98 disappeared and a new singlet corresponding to —OCH_2CONH— in the final F127–$(DFO)_2$ spectra was

observed at δ 3.81 following conjugation to DFO (Figure S2B, Supporting Information). Furthermore, by integrating the peak at δ 3.81 with respect to the doublet corresponding to the polypropylene oxide (PPO) groups of F127 at δ 1.00, it was possible to estimate that around 86% of F127 terminal ends had been capped with DFO and that majority of polymer chains were approximately conjugated to two DFO moieties. To confirm this further, UV–vis was used to measure the percentage of DFO present in F127–$(DFO)_2$ by relying on the well-known absorbance characteristic of the chelator in the presence of iron(III). Since free DFO binds stoichiometrically with iron(III) on the order of 10^{-1} M^{-1} at a 1:1 ratio,[20] its characteristic absorption peak at 430 nm is directly proportional to the concentration of DFO:iron(III) complex present in solution and a linear curve can be easily generated (Figure S3, Supporting Information). Based on this linear equation, the mass fraction of DFO in F127–$(DFO)_2$ (w/w) was 7.23%, which corresponds to a ratio of approximately two DFO moieties per F127 polymer.

TPE was entrapped into F127 and F127–$(DFO)_2$ mixed micelles to form DFO–TFM by the thin-film hydration method. The concentration of the micelles was adjusted to ≈30 mg mL^{-1}, which corresponds to a final concentration of 1×10^{-3} M DFO and 0.012 mg mL^{-1} TPE, respectively. Control F127 micelles (with no DFO conjugated) and encapsulating TPE were also similarly fabricated, termed C-TFM where C stands for control, T for TPE, F for F127, and M for micelle. For the release study, TPE concentration in micelles decreased from 0.012 to 0.0097 mg mL^{-1} at room temperature and to 0.0098 mg mL^{-1} at 37 °C after 48 h, indicating that less than 20% TPE had released at both incubation temperatures (Figure S4, Supporting Information). The morphological structure of micelles was examined by transmission electron microscopy (TEM) and is shown in Figure 2A,B. Essentially DFO–TFM remained spherical in shape with diameters of ≈20 nm before and after chelating with iron(III). Dynamic light scattering (DLS) results also confirmed these findings by revealing a single distinct peak characterized by a z-average diameter of ≈21.1 nm and a polydispersity index (PDI) of 0.125 for DFO–TFM before addition of iron(III) (Figure 2C), and 22.1 nm with a PDI of 0.133 for DFO–TFM after addition of iron(III) (Figure 2D). The incorporation of modified F127–$(DFO)_2$ with F127 to form the final mixed micelles does not appear to disrupt the self-assembly behavior of the poloxamer.

UV–vis measurements were used to confirm the iron chelating properties of DFO–TFM. Solutions containing free DFO, F127–$(DFO)_2$, or DFO–TFM were mixed with excess iron(III) at room temperature and a distinct clear orange color indicative of complex formation immediately formed for all preparations (Figure S5A, Supporting Information). Samples from each solution vial were measured at 430 nm and as expected, no absorption was observed for free DFO or F127–$(DFO)_2$ micelles in the absence of iron(III), although there was slight background absorption in the DFO–TFM solution due to TPE (Figure S5B, Supporting Information). To further rule out the possibility that DFO may only be loosely associated with F127–$(DFO)_2$ and resulting DFO–TFM, each of the three solution vials was washed extensively with a centrifugal filtration unit possessing a molecular weight cutoff (MWCO) of 10 000 Da and the absorbance of the recovered concentrates and filtrates was measured. As revealed in Figure S5A,C (Supporting Information), the absorption peak at 430 nm for the complexes was only observable in the recovered orange concentrates of

F127–$(DFO)_2$ and DFO–TFM but not in their filtrates; in contrast, absorptions at 430 nm were present in both the concentrate and filtrate of free DFO.

TPE is a typical aggregation-induced emission (AIE) dye characterized by strong blue fluorescence in solid state or in poor solvents and no emission when dissolved in good solvents.[21,22] When excited at 350 nm, the fluorescence of TPE in a solution of 90% H_2O and 10% tetrahydrofuran (THF) is characterized by an emission maximum between 450 and 480 nm (Figure 3A). Following its encapsulation into micelles, the fluorescence spectrum of TPE was observed to blue-shift slightly upon excitation and may be attributed to the presence of PPO chains in the core which could interfere with the stacking of TPE molecules and effectively shorten its π-conjugation range.[23] Due to significant overlap between this blue-shifted TPE emission spectrum and the characteristic absorption peak of the DFO:iron(III) complex at ≈430 nm, the fluorescence of TPE can be effectively absorbed and quenched in proportion to the degree of iron(III) chelation to the DFO–TFM. To validate this observation further, the sensitivity of the fluorescence spectrum for an aqueous solution of 30 mg mL^{-1} DFO–TFM was measured in the presence of different concentrations of iron(III) ranging from 0 to 1000×10^{-6} M. As shown in Figure 3B, in the absence of iron(III), exciting DFO–TFM at 350 nm leads to a strong emission spectra for TPE at ≈440 nm. In the presence of iron(III), the fluorescence intensity at 440 nm decreases as the concentration of iron(III) is increased and displays a good a linear relationship within iron(III) concentrations of $1.0 \times 10^{-6} – 1.0 \times 10^{-4}$ M. The detection limit was determined to be 8.3×10^{-7} M (based on $S/N = 3$) (Figure S6, Supporting Information). Optical images of the micelle solutions incubated with varying concentrations of iron(III) were also taken under both ambient and UV illuminations. The vials of solution changed from colorless to orange under ambient lighting, whereas under UV light, the emission color could easily be observed to decrease in intensity from an initial bright fluorescent blue to near colorless with increasing concentrations of iron(III) in solution (Figure S7, Supporting Information). Indeed, these studies have confirmed that DFO–TFM can be utilized as a sensitive turn-off fluorescent sensor for the detection of iron(III) at micromolar concentrations.

The DFO–TFM system is expected to show high selectivity to iron(III) because of the unique absorbance of DFO for binding iron(III) at 430 nm (Figure S8A, Supporting Information). To verify this, different metal cations including Ag(I), Ni(II), Mn(II), Cu(II), Co(II), Mg(II), Zn(II), Ca(II), K(I), Na(I), Hg(II), Al(III), Cr(III), and Ga(III) were incubated with the DFO–TFM. UV–vis scanning experiments were first conducted to investigate the potential absorbance response of DFO–TFM to other metal ions. As shown in Figure S8B (Supporting Information), the strongest absorbance peak was noted only for DFO–TFM incubated with iron(III) followed by a lower absorbance peak for iron(II) at 430 nm. It should be noted that the iron(II) absorbance peak observed was likely due to DFO chelation to iron(III) resulting from atmospheric oxidation of iron(II) to iron(III) in solution.[24] There were no other significant absorbance peaks observed with other metal ions investigated. Since the DFO–TFM absorbance intensity change at 430 nm was the greatest for iron(III), only iron(III) is capable of efficiently quenching the fluorescence of TPE in micelles when excited at 350 nm (Figure 3C). None of the other metal ions resulted in fluorescence quenching and iron(II) only had a slight effect due to presence of iron(III) from atmospheric oxidation.

Competition experiments were carried out by first chelating iron(III) with micelles and then adding either 1× or 50× equivalents of other potentially competing metal ions to the solution. It can be observed that only 50× equivalents of Ga(III) can slightly increase the corresponding fluorescence intensity (Figure 3D). The displaced chelated iron(III) also manifested a decrease in the absorbance intensity ratio (Figure S9, Supporting Information). Apart from Ga(III), the presence of all other metal ions investigated does not interfere with iron(III) binding to the micelle or subsequent fluorescence quenching. The disturbance by Ga(III) is due to the strong binding constant of DFO to Ga(III) (10^{28} M^{-1}),[25] which is slightly lower than that of iron(III) but still significantly strong. Since Ga(III) concentration in the body is negligible due to its lack of biological function in eukaryotic cells other than to disturb iron metabolism when exogenously introduced, the DFO–TFM system is unlikely to be affected when used to monitor iron overload conditions.

Although DFO is frequently used to treat iron-overload conditions, the clinical use of the drug is hindered due to its cytotoxicity issues which can be minimized through its incorporation into appropriately designed nanomaterials. Here, iron overloaded or non-iron overloaded mouse J774A.1 macrophage cells were treated with equivalent amounts of free DFO or DFO–TFM ranging from 0.05×10^{-6} to 1000×10^{-6} M and allowed to incubate for 48 h prior to assessing cytotoxicity. The result of the metabolism-based resazurin assay shows that DFO–TFM was 100-fold less toxic compared to free DFO in non-iron overloaded cells, with 50% viability for DFO at concentration as low as $\approx 8 \times 10^{-6}$ M compared to DFO–TFM at $\approx 800 \times 10^{-6}$ M (Figure 4A). Similar results were obtained in iron-overloaded J774A.1 cells, where free DFO inhibited 50% cell viability at $\approx 11 \times 10^{-6}$ M compared to DFO–TFM which inhibited 50% cell viability at 1.0×10^{-3} M equivalent DFO concentration (Figure 4B). In contrast, the C-TFM which contained no DFO was not toxic to either iron overloaded or non-iron overloaded J774A.1 cells. The toxicity of DFO at high concentrations is hypothesized to be due to the chelation of too much iron away from critical intracellular proteins which can disrupt metabolic and cellular respiration processes. Next, as shown in Figure 4C, 100×10^{-6} M ferric ammonium citrate (FAC) was added to J774A.1 macrophage cells for 24 h to induce cellular ferritin expression (from 4.19 ng μg^{-1} total protein to 10.58 ng μg^{-1} total protein, $p < 0.001$) prior to addition of chelating treatments. The results of the quantitative colorimetric enzyme-linked immunosorbent assay (ELISA) reveal that at the lower dose of 10×10^{-6} M, both free DFO (4.29 ng μg^{-1} total protein, 59.5% decrease, $p < 0.001$) and DFO–TFM (4.78 ng μg^{-1} total protein, 54.8% decrease, w had similar treatment effects (ns) with ferritin returning to non-iron overloaded control baseline levels; however, at a higher dose of 50×10^{-6} M, the ferritin concentration decreased below normal baseline level (2.80 ng μg^{-1} total protein for DFO or 73.5% decrease, $p < 0.001$ and 3.24 ng μg^{-1} total protein for DFO–TFM or 69.4% decrease, $p < 0.001$) and is indicative of too much iron being chelated. Therefore, monitoring the chelation process to prevent excess iron removal (as indirectly quantified by ferritin concentration[26]) is very important for clinical applications due to the critical role iron plays in maintaining cellular function.

Excess iron is always stored in ferritin to help maintain the balance of iron, especially in iron-overloaded cells. Ferritin is a ubiquitous intracellular protein responsible for storing iron and releasing it in a controlled fashion as needed by many cells of the body.[27]

However, current molecular and supramolecular fluorescent sensors have been mostly developed to selectively detect only exogenous iron(III) added for a few hours at most to live cells and does not reflect the actual state of iron overload in the cell.[11] Moreover, monitoring the iron chelation process to avoid excess iron removal is significantly needed for practical application. The unique physical properties of DFO and its ability to chelate iron from ferritin,[28] coupled with its favorable absorbance and fluorescence turn-off response at ≈430 nm in the presence of encapsulated TPE permits the possibility of using DFO–TFM to visually monitor the degree of iron-overload in living cells. J774A.1 cells were treated with 0, 50×10^{-6}, and 100×10^{-6} M FAC and allowed to incubate for 24 h to induce ferritin expression and mimic various degrees of iron-overload (Figure S10, Supporting Information). After that, the cells were supplemented with 1 mg mL^{-1} of DFO–TFM solution for 1 h at 37 °C and washed with phospate-buffered saline (PBS). The lysosomes were stained by incubating cells with LysoTracker Deep Red for 30 min before confocal laser scanning microscopy (CLSM) imaging. As shown in Figure S11 (Supporting Information), strong and bright fluorescence images were observed by CLSM in non-iron overload cells (0 μM FAC added), and corresponds to normal ferritin expression levels. In contrast, the fluorescence of TPE significantly decreased when DFO–TFM was incubated with J774A.1 cells that had been treated with 50×10^{-6} M FAC and this effect was even more pronounced in cells that had been treated with 100×10^{-6} M FAC. Colocalization of images indeed verified that DFO–TFM were endocytosed by cells and trafficked to lysosomes where a vast majority of excess ferritin can be found when cells become iron-overloaded.

DFO–TFM can also be used to monitor the chelation process in iron-overloaded cells. After treating cells with 50×10^{-6} M FAC for 24 h to induce ferritin expression, cells were incubated with DFO–TFM for 1 h and then replaced with fresh culture medium for 1 or 10 h, respectively. Compared to C-TFM micelles with no DFO conjugation and therefore no iron chelation capabilities (Figure 5A), J774A.1 cells treated with DFO–TFM exhibited significantly weaker fluorescence after 10 h incubation compared to 1 h (Figure 5B) due to gradual chelation of iron by DFO–TFM from ferritin in lysosomes over time. For C-TFM, there was no obvious difference between the fluorescence at the 1 and 10 h time points. Furthermore, J774A.1 cells remained healthy during the entire incubation period across all the studies conducted and validate the low cytotoxicity of the system. We have demonstrated that DFO–TFM is able to distinguish between various iron-overload states in cells and can be used to monitor the chelation process as a function of time in living cells.

In summary, multifunctional self-assembled polymeric micelles were developed and investigated for chelation and selective detection of iron(III) in vitro and in iron-overloaded cells. TPE was encapsulated into the micelle core and the iron chelate drug DFO was conjugated to micelles to generate a fluorescence quenching detection system. The key to the successful formation of this fluorescence quenching system is due to the near-ideal overlap between the absorption spectrum of the DFO:iron(III) complex and fluorescence spectrum of TPE. The DFO–TFM micelles also retained the iron-chelation properties of DFO and exhibited negligible cytotoxicity compared to free DFO. Furthermore, this fluorescence “turn-off” system can be utilized to detect the presence of iron and to monitor the chelation process in an iron overload cell model. This study serves as an effective proof-

of-concept model for designing future in vivo systems capable of combining the features of iron chelation with iron detection; efforts toward the development of such detection systems are currently underway.

Supplementary Material

Refer to Web version on PubMed Central for supplementary material.

Acknowledgments

This work was supported by the NIH grant R01DK099596 awarded to M.P.X.

References

1. Zecca L, Youdim MB, Riederer P, Connor JR, Crichton RR. Nat Rev Neurosci. 2004; 5:863. [PubMed: 15496864]
2. Barnham KJ, Bush AI. Chem Soc Rev. 2014; 43:6727. [PubMed: 25099276]
3. Brittenham GM. N Engl J Med. 2011; 364:146. [PubMed: 21226580]
4. Poggiali E, Cassinerio E, Zanaboni L, Cappellini MD. Blood Transfus. 2012; 10:411. [PubMed: 22790257]
5. Levine JE, Cohen A, MacQueen M, Martin M, Giardina PJ. J Pediatr Hematol/Oncol. 1997; 19:139.
6. Liu Z, Lin TM, Purro M, Xiong MP. ACS Appl Mater Interfaces. 2016; 8:25788. [PubMed: 27623539]
7. Liu Z, Wang Y, Purro M, Xiong MP. Sci Rep. 2016; 6:20923. [PubMed: 26868174]
8. ul-haq MI, Hamilton JL, Lai BFL, Shenoi RA, Horte S, Constantinescu I, Leitch HA, Kizhakkedathu JN. ACS Nano. 2013; 7:10704. [PubMed: 24256569]
9. Sahoo SK, Sharma D, Bera RK, Crisponi G, Callan JF. Chem Soc Rev. 2012; 41:7195. [PubMed: 22885471]
10. Zhu H, Fan JL, Wang BH, Peng XJ. Chem Soc Rev. 2015; 44:4337. [PubMed: 25406612]
11. Carter KP, Young AM, Palmer AE. Chem Rev. 2014; 114:4564. [PubMed: 24588137]
12. Fleming RE, Ponka P. N Engl J Med. 2012; 366:348. [PubMed: 22276824]
13. Kataoka K, Harada A, Nagasaki Y. Adv Drug Delivery Rev. 2012; 64:37.
14. Gaucher G, Dufresne MH, Sant VP, Kang N, Maysinger D, Leroux JC. J Controlled Release. 2005; 109:169.
15. Batrakova EV, Kabanov AV. J Controlled Release. 2008; 130:98.
16. Nasongkla N, Bey E, Ren JM, Ai H, Khemtong C, Guthi JS, Chin SF, Sherry AD, Boothman DA, Gao JM. Nano Lett. 2006; 6:2427. [PubMed: 17090068]
17. Zhang W, Shi YA, Chen YZ, Ye JA, Sha XY, Fang XL. Biomaterials. 2011; 32:2894. [PubMed: 21256584]
18. Huang CK, Lo CL, Chen HH, Hsiue GH. Adv Funct Mater. 2007; 17:2291.
19. Araki J, Zhao CM, Kohzo I. Macromolecules. 2005; 38:7524.
20. Keberle H. Ann N Y Acad Sci. 1964; 119:758. [PubMed: 14219455]
21. Hong YN, Lam JWY, Tang BZ. Chem Soc Rev. 2011; 40:5361. [PubMed: 21799992]
22. Hong YN, Lam JWY, Tang BZ. Chem Commun. 2009:4332.
23. Qiao J, Liu Z, Tian Y, Wu M, Niu ZW. Chem Commun. 2015; 51:3641.
24. Goodwin JF, Whitten CF. Nature. 1965; 205:281. [PubMed: 14270711]
25. Wadas TJ, Wong EH, Weisman GR, Anderson CJ. Chem Rev. 2010; 110:2858. [PubMed: 20415480]
26. Lipschitz DA, Cook JD, Finch CA. N Engl J Med. 1974; 290:1213. [PubMed: 4825851]
27. De Domenico I, Ward DM, Kaplan J. Nat Rev Mol Cell Biol. 2008; 9:72. [PubMed: 17987043]

28. Crichton RR, Roman F, Roland F. J Inorg Biochem. 1980; 13:305. [PubMed: 7193239]

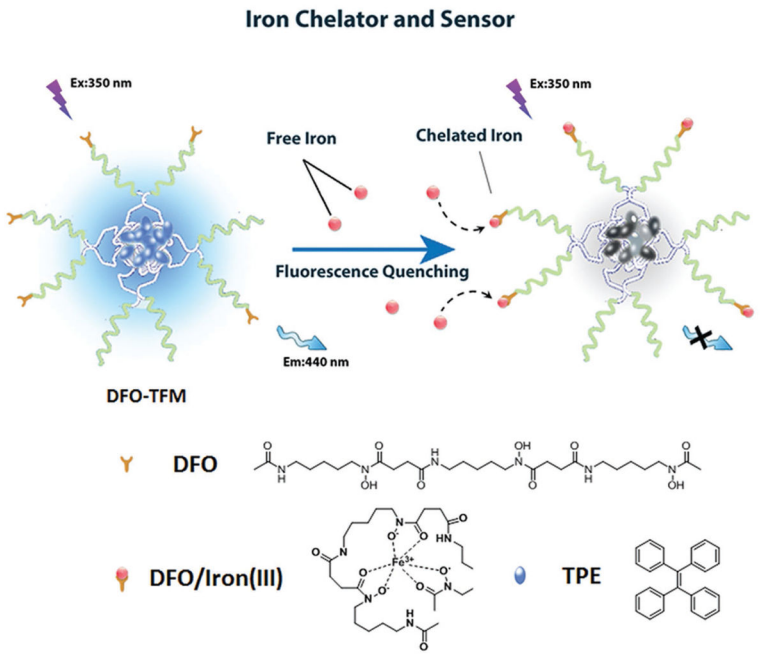

Figure 1.
Formation of the DFO–TFM and its selective turn-off fluorescence sensing properties in the presence of iron(III).

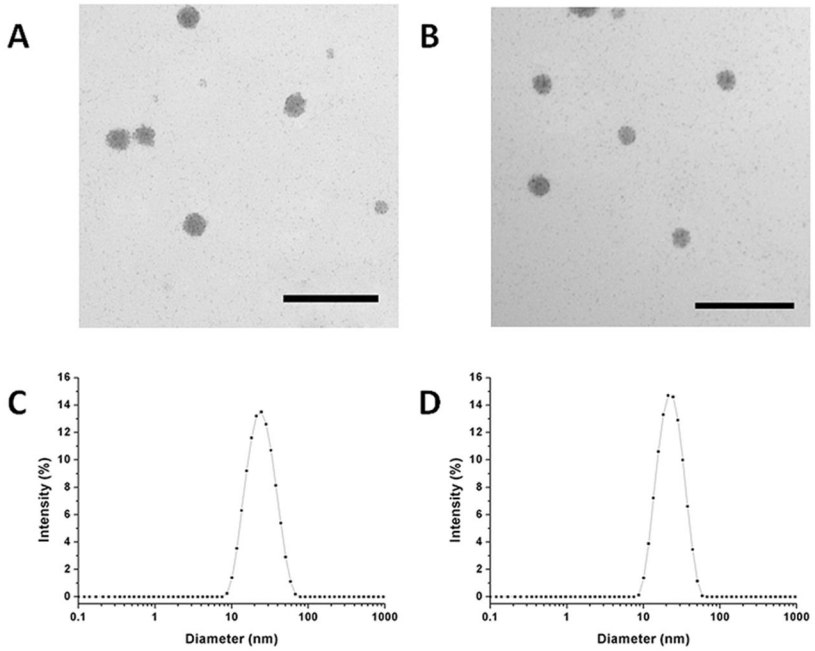

Figure 2.

Representative TEM image of DFO–TFM A) before and B) after combining with iron(III); DLS size distribution of DFO–TFM C) before and D) after combining with iron(III) in Tris/HCl buffer. The TEM scale bar represents 100 nm.

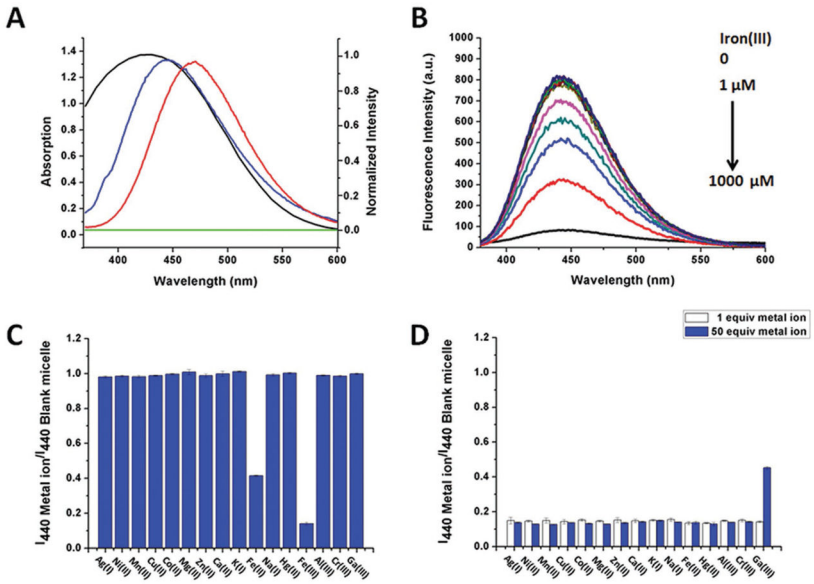

Figure 3.

A) Fluorescence spectra (λ_{exc}: 350 nm) of C-TFM (blue line) and TPE in 90% H_2O/THF (red line); the absorption spectra of DFO in the absence (green line) and presence (black line) of iron(III). B) Fluorescence spectra (λ_{exc}: 350 nm) of DFO–TFM upon titration of iron(III). C) Fluorescence intensity changes ([$I_{440\ Metal\ ion}/I_{440\ Blank\ micelle}$]) of DFO–TFM upon addition of Ag (I), Ni(II), Mn(II), Cu(II), Co(II), Mg(II), Zn(II), Ca(II), K(I), Na(I), Fe(II), Hg(II), Fe(III), Al(III), Cr(III), or Ga(III), respectively (λ_{exc}: 350 nm); Results are presented as mean ± SD (n = 3). D) Fluorescence intensity changes ([$I_{440\ Metal\ ion}/I_{440\ Blank\ micelle}$]) of DFO–TFM prechelated to Fe(III) in the presence of 1× or 50× equivalence of Ag(I), Ni(II), Mn(II), Cu(II), Co(II), Mg(II), Zn(II), Ca(II), K(I), Na(I), Fe(II), Hg(II), Al(III), Cr(III), and Ga(III), respectively (λ_{exc}: 350 nm); Results are presented as mean ± SD (n = 3).

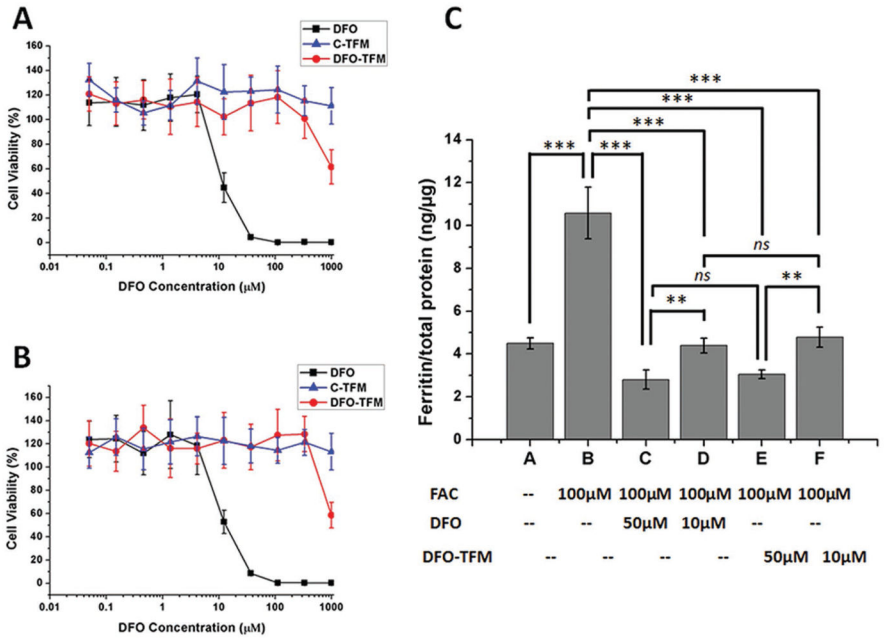

Figure 4.

Cytotoxicity of free DFO, C-TFM, and DFO–TFM in A) non-iron overloaded and B) iron overloaded J774A.1 cells after 48 h incubation; a representative set of data is shown where each data point is presented as the mean ± SD ($n = 3$). C) Ferritin reduction assay to monitor iron chelation efficacy of DFO and DFO–TFM in iron overloaded J774A.1 cells (iron overload was induced by 24 h incubation with 100×10^{-6} M FAC); cells were treated with DFO or DFO–TFM at 10×10^{-6} or 50×10^{-6} M for 48 h and cellular ferritin level was measured by a mouse ferritin ELISA assay. Results are normalized to total protein (ng μg^{-1}) and presented as mean ± SD ($n = 3$). “ns” means the difference was not significant, ** $p < 0.01$, *** $p < 0.001$.

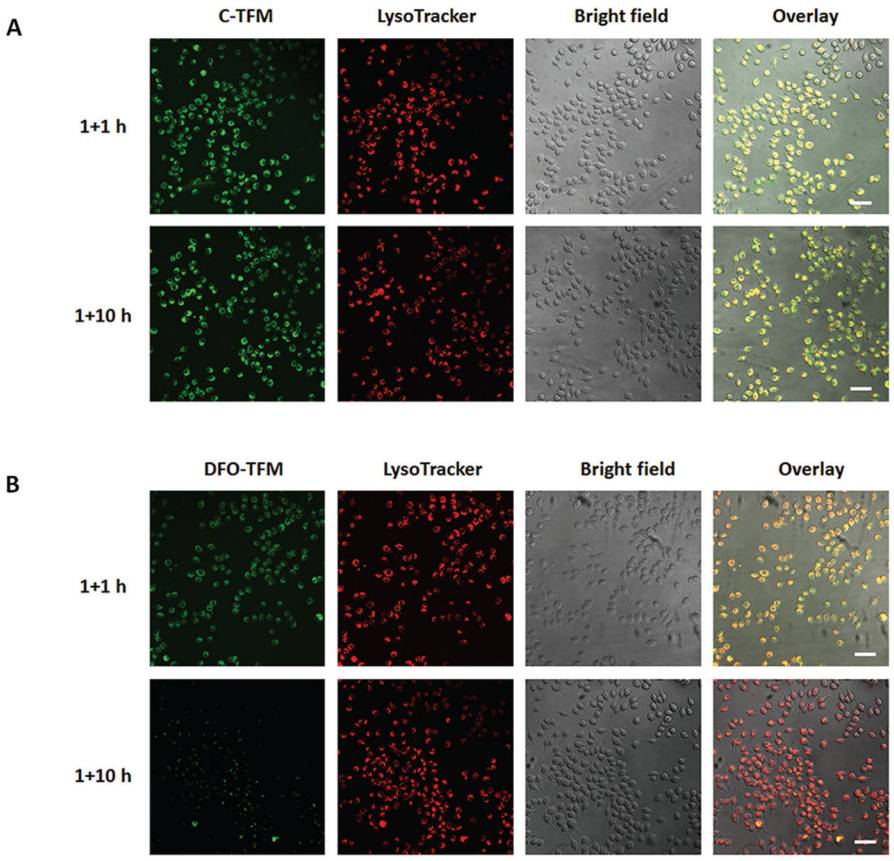

Figure 5.

Fluorescence images of J774A.1 cells pretreated with 50×10^{-6} M FAC to induce iron-overload and ferritin overexpression. Next, cells were incubated with A) C-TFM and B) DFO–TFM for 1 h, and replaced with culture medium for an additional 1 or 10 h incubations. Images from left to right correspond to micelle fluorescence, LysoTracker fluorescence, bright field, and overlaid images (scale bars: 50 μm).